JOURNAL OF MATERIALS SCIENCE 33 (1998) 3867–3874

Cyclic fatigue crack growth behaviour in β-(Si–Al–O–N) at ambient and elevated temperatures

GUO-DONG ZHAN
The State Key Laboratory of High Performance Ceramics and Superfine Microstructure, Shanghai Institute of Ceramics, Chinese Academy of Sciences, Shanghai 200050, People's Republic of China

M. J. REECE, MING LI, J. M. CALDERON-MORENO
Department of Materials, Queen Mary and Westfield College, University of London, London E1 4NS, UK
E-mail: m.reece@qmw.ac.uk

Four-point bending fatigue tests on a hot-pressed sintered Sm–β-(Si–Al–O–N) ceramic were conducted at room temperature, 900 °C and 1000 °C in air under different load ratios and cyclic frequencies. The growth of indentation cracks was measured during the fatigue tests. The results indicate that the cyclic fatigue crack growth threshold is lower and crack growth rates are higher, for given values of K_{max}, at 1000 °C than those at room temperature. The cyclic fatigue crack growth behaviour at 900 °C is similar to that at room temperature. It was found that the crack growth retardation due to cyclic fatigue loading is much more pronounced at higher frequencies. An increase in cyclic frequency from 1 to 10 Hz cause a reduction of up to two orders of magnitude in crack propagation rates. High-temperature cyclic fatigue crack growth rates increased and threshold stress intensity factor ranges decreased with increasing load ratio. Possible mechanisms for cyclic crack growth are discussed.

1. Introduction

Indentation cracks are widely used to investigate fracture processes and properties in brittle materials. In the past, most studies of indentation fracture have been restricted to the measurement of fracture toughness of ceramic materials [1, 2]. Controlled surface flaws loaded in bending were first employed by Petrovic *et al.* [3] and Mendiratta and Petrovic [4] to study the static fatigue crack growth behaviour of a hot-pressed Si_3N_4 almost two decades ago. Recently, Liu *et al.* [5], Liu and Chen [6] and Zhan *et al.* [7] have also reported the static and cyclic fatigue crack growth behaviour of hot-pressed Si_3N_4 [5] and α–β-(Si–Al–O–N) (sialon) [7] ceramic materials at elevated temperatures using multiple controlled surface flaws. For a hot-pressed Si_3N_4 [5] with 70 vol% (elongated) β-Si_3N_4 and 30 vol% (equiaxed) α-sialon, the crack growth rate at 1400 °C was slower under cyclic loading than under sustained loading, even after the effect of load-time profile was accounted for. For α–β-sialon, the static and cyclic fatigue crack growth rates at 1200 °C showed three characteristic regions [7]. In the lower-stress-intensity-factor region, the cyclic fatigue crack growth rate was slower than for static fatigue at the same stress intensity factor. At higher stress intensities, the crack growth rates for both static and cyclic fatigue were almost the same. These observations are consistent with the longer lifetime under cyclic loading compared with sustained loading at high temperatures which has been reported in the literature [8–20]. This behaviour is different from room-temperature cyclic fatigue behaviour of ceramics where cyclic loading enhances fatigue crack growth [22–33].

Several reports in the literature have been concerned with the micromechanisms of elevated-temperature subcritical crack growth for structural ceramics [15, 16, 18–21]. The single-edge-notched specimens, with relatively long crack lengths (100–1000 μm, typically) have been extensively used to measure subcritical crack growth rates at high temperatures. The present investigation characterized the subcritical crack growth behaviour of relatively short cracks (less than 500 μm) in sialon using multiple "controlled" surface flaws. Controlled flaws in the form of semi-elliptical cracks with a range of sizes were introduced by Vickers microhardness indentation. The dimensions of the controlled cracks were of a similar but generally longer length than natural flaws (less than 100 μm). They therefore simulated the subcritical crack growth behaviour of natural flaws. A number of non-interacting controlled flaws (typically eight) were produced within the centre span of each test specimen, to maximize the fatigue data generated by each experiment.

The purpose of this experimental study was to characterize the high-temperature cyclic fatigue crack growth behaviour of 100 vol% β-sialon under different stress ratios and different cyclic frequencies. Tests were conducted in both static and cyclic tension loading at room temperature, 900 °C and 1000 °C. A direct comparison of cyclic fatigue crack growth results under different experimental conditions provides some insight into the failure mechanisms in ceramics at room and high temperatures.

2. Material and experimental methods

2.1. Material

The starting powders used in this study were Si_3N_4 (88.0 mass%), AlN (6.0 mass%), Al_2O_3 (3.0 mass%) and Sm_2O_3 (3.0 mass%). The mixtures of powders were milled in ethanol for 24 h in an alumina jar, using sintered silicon nitride grinding media. After the powder mixtures were dried, they were die pressed into bars under 20 MPa uniaxial pressure and then isostatically pressed at 290 MPa. Pressed compacts were placed in a covered graphite crucible with a protective powder bed of 90 mass% Si_3N_4 + 10 mass% BN, hot pressed at 1750 °C in N_2 for 0.5 h to reach full density and then heat treated at 1550 °C for 6 h to obtain pure β-sialon. Scanning electron microscopy examination revealed a microstructure containing elongated β-sialon grains surrounded by grain boundary phases (Fig. 1). The material is of interest because of its good oxidation resistance and good high-temperature mechanical properties. X-ray diffraction analysis of the sample further confirmed that the phase compositions of the sample was predominantly β-sialon with no detected α-sialon but with some crystallized grain boundary phases. The properties of β-sialon ceramic used in this study are shown in Table I.

2.2. Experimental methods

Specimens were prepared as rectangular bend bars with dimensions of 37 mm × 4 mm × 3 mm. The tensile surface of the specimens were finely ground along the long axis, and then polished using diamond paste down to 1 μm particle size to obtain a good surface finish. A series of Vickers indentations were introduced on the tensile surface using a range of indentation loads (10–30 kgf). These indents were spaced 1.0 mm apart and carefully aligned so that the radial cracks emanating from the corners of the indentations were all parallel or perpendicular to the long axis of the specimen. Cyclic four-point bending fatigue tests were conducted using a commercial servohydraulic machine (Instron 8500) operated under load control, with a sinusoidal wave form at frequencies of 1 Hz and 10 Hz and load ratios R (minimum load-to-maximum load ratio) of 0.1 and 0.3, respectively. An alumina four-point bending configuration with an inner span of 10 mm and an outer span of 30 mm was used. The specimens were heated to the test temperature at a rate of 15 °C min^{-1}, held for 15 min and then slowly loaded until the test stress level was reached. The tests were performed with loading times of 30–60 min; then the load was removed and the furnace was cooled. Because the test time was very short and the temperatures relatively low, the effect of creep deformation was considered to be negligible. This was confirmed by the fact that the tested specimens were flat and showed no measurable curvature caused by creep deformation. Any curvature of the specimens within the resolution that we could have detected would have only produced a very small correction to the estimated stresses (less than 1%). The surface indentation crack lengths were measured using an optical microscope at a magnification of 300×. When the specimen did not fail during high-temperature testing, a room-temperature fracture test was conducted. For comparison, static fatigue tests at the same temperature and maximum stress were also conducted. Following completion of these tests, the fracture surfaces were examined with a scanning electron microscope in order to measure the size and shape of the initial and the critical crack. The applied stress intensity factor at the crack tip subjected to pure bending was calculated from the finite-element analysis of Newman and Raja [23] for semielliptical surface cracks in terms of crack depth, a, half-surface-crack length, c, specimen thickness, t, specimen width, b, geometric factors, Q, S and M, H, and remote (outer surface) bending stress, σ_a:

$$K_{app} = \frac{MSH}{Q}\,\sigma_a(\pi a)^{1/2} \quad (1)$$

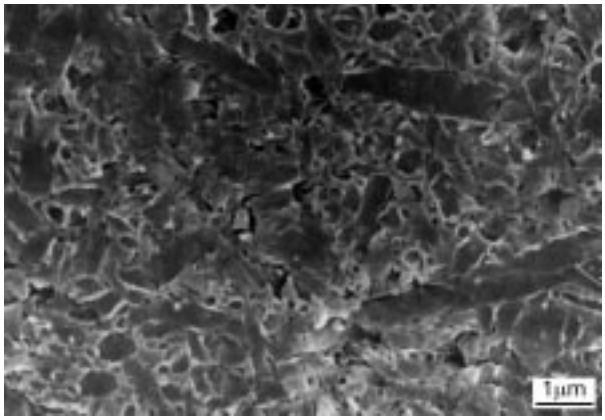

Figure 1 Microstructure of as-received hot-pressed β-sialon revealed by plasma etching showing elongated β-sialon grains with some crystallized grain boundary phases.

TABLE I Properties of Sm–β-sialon ceramic used in this study

Young's Modulus, E (GPa)	Vickers hardness, H_v (GPa)	Flexural strength (MPa)		Fracture toughness, K_{Ic} (MPa $m^{1/2}$)
		25 °C	1300 °C	
350	15.99	800	600	8.6 ± 1.0

where H is the bending multiplier given by

$$H = 1 - \left(0.34 + 0.11\frac{a}{c}\right)\frac{a}{t} \quad (1a)$$

and M, S and Q are geometric functions given by

$$M = \left(1.13 - 0.99\frac{a}{c}\right) + \left[-0.54 + 0.89\left(0.2 + \frac{a}{c}\right)^{-1}\right]\left(\frac{a}{t}\right)^2 + \left[0.5 - \left(0.65 + \frac{a}{c}\right)^{-1} + 14\left(1 - \frac{a}{c}\right)^{24}\right]\left(\frac{a}{t}\right)^4 \quad (1b)$$

$$S = \left[1.1 + 0.35\left(\frac{a}{t}\right)^2\right]\left(\frac{a}{c}\right)^{0.5} \quad (1c)$$

$$Q^2 = 1 + 1.464\left(\frac{a}{c}\right)^{1.65} \quad (1d)$$

The aspect ratio, c/a, for the semielliptical crack was approximated using an empirical equation recommended by ASTM Standard E740 [24]:

$$\frac{a}{c} + \frac{a}{t} = 1 \quad (2)$$

The indentation fracture mechanics concerning an indentation and its associated elastic–plastic deformation has been developed by Marshall and Lawn [22]. A median crack or Palmqvist crack can be formed by Vickers indentation. Which type of crack system forms depends on the combination of material parameter, E/H, and applied load. Residual stresses remain owing to the indentation plastic deformation zone. In the case of silicon-nitride-based ceramics, the formation of median cracks is dominant. The residual stress intensity factor, K_{res}, from the residual crack-opening stress was calculated in terms of indentation load, P, and the half-crack length, c, by [22]

$$K_{res} = \chi\left(\frac{E}{H}\right)^{1/2}\frac{P}{c^{3/2}} \quad (3)$$

where the pre-factor, χ, is a geometric factor. To investigate whether the indentation residual stresses were annealed at high temperatures, the results of identical room-temperature fatigue tests performed on indentations in as-received specimens and specimens heat treated at 1250 °C for 1 h and slightly polished were compared. The experimental results shown in Fig. 2 indicated that the residual stresses were not significantly reduced by heat treatment at 1250 °C and therefore at the lower test temperatures, 900 and 1000 °C. Thus, the total stress intensity factor, K_I, at the crack tip at all the test temperatures was given by the summation of Equations 1 and 3, i.e.,

$$K_I = K_{app} + K_{res} \quad (4)$$

We assumed that the time-based fatigue crack growth rate, da/dt, was a function of the total stress intensity factor and could be expressed by the equation

$$da/dt = A(K_I)^n \quad (5)$$

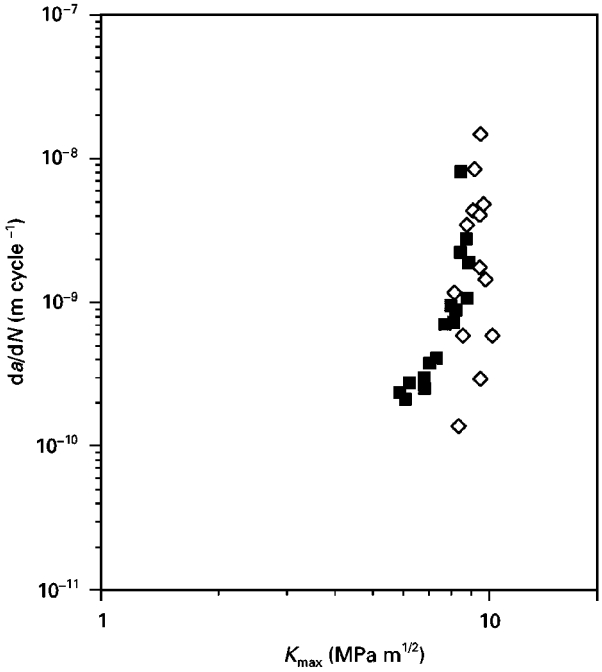

Figure 2 Relationship between fatigue crack growth rate, da/dN, and maximum stress intensity factor, K_{max}, for β-sialon ceramic subjected to cyclic tension loading at room temperature with heat treatment at 1250 °C (■) and without heat treatment (◇).

where A and n are constants, which can be obtained by least-squares fitting of the measured crack growth data, and K_I is the stress intensity factor at the crack tip. The conventional averaging method was used, i.e., the average crack growth rate for each indent was obtained by dividing the total crack extension by the test duration, and the average stress intensity factor was the mean value of the stress intensity factors associated with the initial and final crack lengths. For cyclic fatigue, K_I was replaced by K_{max}, the maximum K experienced by the crack tip during cyclic loading, so that

$$\frac{da}{dN} = C(K_{max})^m \quad (6)$$

Because of the positive K_{res} term, the stress intensity factor ratio, K_{min}/K_{max}, will always be greater than the load ratio, R. The load ratio was constant during the experiments. However, the stress intensity factor ratio decreased during the experiments because K_{res} decreased as the cracks grew. For convenience the load ratio has been used to define the conditions of the cyclic fatigue tests.

3. Results and discussion

3.1. Temperature dependence

The fatigue crack growth behaviour of Sm–β-sialon ceramic under cyclic loading at different temperatures and $R = 0.3$ is shown in Fig. 3 in terms of the growth rate per cycle as a function of the maximum stress intensity factor. The fitting parameters, m and C, for the Paris relation are listed in Table II. The cyclic fatigue crack growth behaviour at temperatures from

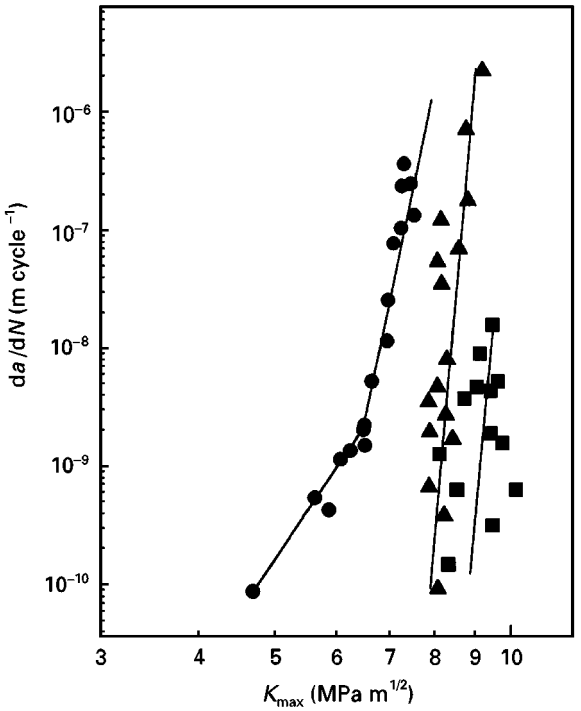

Figure 3 Relationship between fatigue crack growth rate, da/dN, and maximum stress intensity factor, K_{max}, for β-sialon ceramic subjected to cyclic tension loading at room temperature (25 °C) (■), 900 °C (▲) and 1000 °C (■) and cyclic frequency of 10 Hz and load ratio of 0.3.

25 to 900 °C show similar characteristics. However, the cyclic fatigue crack growth threshold is significantly lower and the crack growth rates higher at 1000 °C than those at room temperature. This behaviour is similar to results reported previously for the high-temperature behaviour of ceramics [19, 20].

3.2. Frequency effect

Fig. 4a shows the variation in the fatigue crack growth rate, da/dN, with the maximum stress intensity factor, K_{max}, for tests conducted at 1000 °C at the same load ratio ($R = 0.1$) but different frequencies, f, Fig. 4a shows that, at $R = 0.1$, an increase in cyclic frequency from 1 to 10 Hz causes a reduction of up to two orders of magnitude in crack propagation rates. This behaviour is similar to the trend generally exhibited by other ceramics at high temperatures [5, 8, 15]. The variation in the crack velocity, da/dt, for static loading at 1000 °C with a sustained stress intensity factor, K_I, is plotted in Fig. 4b. For comparison, the cyclic fatigue crack growth per unit time is defined as

$$\frac{da}{dt} = \frac{da}{dN} f \tag{7}$$

and the maximum stress intensity factor is given by

$$K_{max} = \frac{\Delta K}{1 - R} \tag{8}$$

It can be seen that the crack growth retardation due to cyclic fatigue loading is much more pronounced at higher frequencies. If we assume that crack growth was controlled by the same mechanism under static and cyclic fatigue, the static fatigue crack growth rate, V_s can be predicted from cyclic fatigue data, V_c using

TABLE II Experimental conditions and material parameters for fatigue crack growth for various materials

Material	Temperature of testing (°C)	R	f (Hz)	ΔK range (MPa m$^{1/2}$)	C (m cycle (MPa m$^{1/2}$)^m)	m	Reference
90% pure Al_2O_3	1050	0.15	2.0	2.6–4.8	6.3×10^{-11}	8.0	[18]
Al_2O_3–33 vol% SiC_w	1400	0.15	2.0	3.5–5.5	4.0×10^{-10}	3.7	[17]
Si_3N_4 + 10 vol% SiC_w	1400	0.1	10	3.0–6.0	2.6×10^{-13}	9.13	[14]
α-sialon + β-Si_3N_4	1400	0.1	0.1	—	1.8×10^{-11}	4.25	[5]
	1400	0.1	1	—	5.96×10^{-12}	5.16	[5]
	1400	0.1	5	—	2.76×10^{-13}	8.18	[5]
(Mo, W) S_2 + 30 vol% SiC_p + 2 wt% C	1300	0.2	10	4.6–7.0	1.8×10^{-11}	3.8	[15]
(Mo, W) S_2 + 30 vol% SiC_p	1200	0.2	10	4.1–8.0	3.3×10^{-12}	3.9	[15]
	1300	0.2	10	2.1–4.7	2.3×10^{-10}	6.0	[15]
α–β-sialon	1200 (region I)	0.1	5	2.0–2.3	7.13×10^{-17}	22.0	[7]
	1200 (region II)	0.1	5	2.3–3.23	2.33×10^{-9}	4.01	[7]
	1200 (region III)	0.1	5	3.23–3.75	1.3×10^{-21}	27.6	[7]
β-sialon	25	0.3	10	—	5.03×10^{-36}	33	Present study
	900	0.3	10	—	9.8×10^{-35}	30	Present study
	1000	0.3	10	—	3.95×10^{-26}	26	Present study
	1000	0.1	10	—	9.2×10^{-29}	23	Present study
	1000	0.1	1	—	4.8×10^{-22}	17	Present study
	1000	1	0	—	2.82×10^{-37}	100	Present study
TiB_2–SiC	750	0.1	2	—	2.97×10^{-27}	35	[16]
	800	0.1	2	—	9.44×10^{-28}	35	[16]
	850	0.1	2	—	4.58×10^{-31}	37	[16]

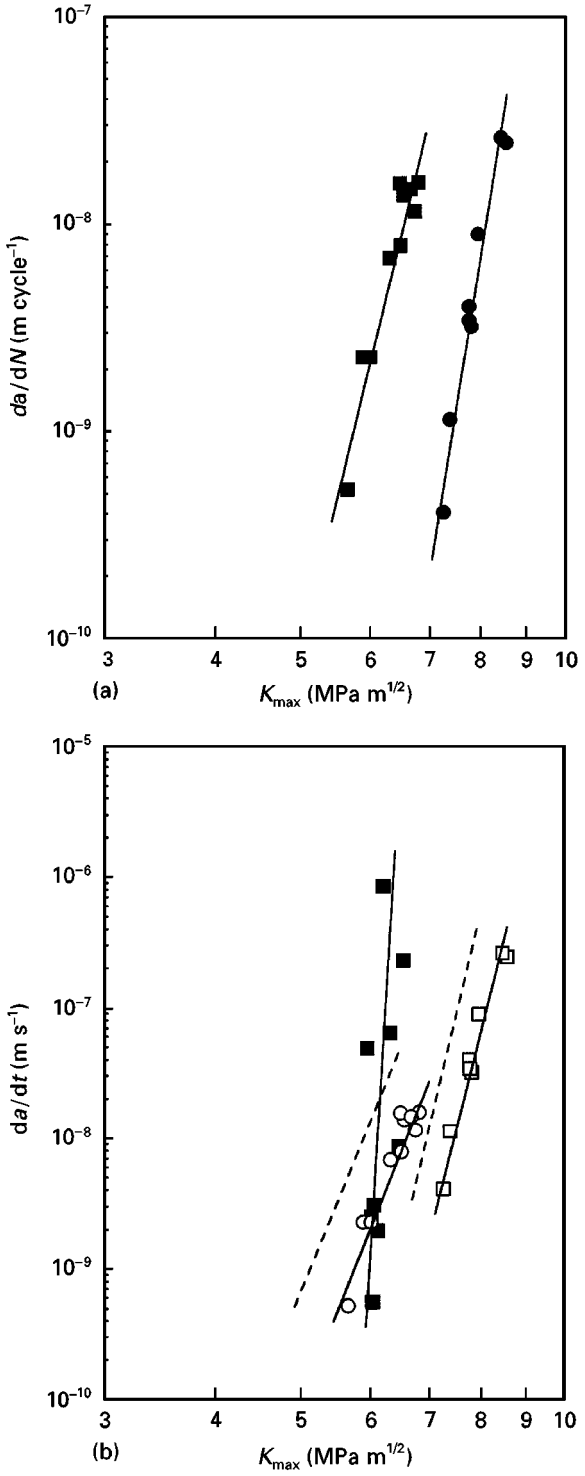

Figure 4 (a) Variation in the fatigue crack growth rate, da/dN, with the maximum stress intensity factor, K_{max}, for tests conducted at 1000 °C at the same load ratio ($R = 0.1$) but different frequencies ($f = 1$ Hz (■) and $f = 10$ Hz (●)). (b) Variation in crack growth velocity, da/dt, as a function of sustained stress intensity factor, K_I for static crack growth ($R = 1$) in β-sialon ceramic at 1000 °C (■). Also shown are the cyclic fatigue crack growth velocities, da/dt = (da/dN) f, as a function of the maximum stress intensity factor for frequencies of 1 Hz (○) and 10 Hz (□) and load ratio, $R = 0.1$. The broken lines represent predicted static fatigue crack growth rate based on the cyclic fatigue data.

the following equation:

$$\frac{V_c}{V_s} = \frac{\left(\int_0^f \sigma_c^n(t)\,dt\right)}{\sigma_s^n} \qquad (9)$$

where f is the cyclic test frequency, $\sigma_c(t)$ is the time-dependent applied stress during cyclic loading and σ_s is the static stress. The broken lines in Fig. 4b represent predicted static crack growth rate from cyclic data (using $R = 0.1$), and it is clearly not comparable with the experimental results, especially at high frequency. This is an overestimate of the correction required since K_I has a contribution from K_{res} which effectively increases the stress intensity factor ratio, K_{min}/K_{max}, compared with R, and therefore the true correction factor would be even smaller than shown. These observations indicate that the crack growth mechanism of high-temperature cyclic fatigue at higher frequencies is different from that of static fatigue and therefore it is not simply just time and effective stress dependent.

3.3. Effect of load ratios

The fatigue crack growth behaviour of Sm–β-sialon ceramic at 1000 °C under cyclic loading at different load ratios is shown in Fig. 5a in terms of the growth rate per cycle as a function of the stress intensity range, ΔK. It can be seen that the cyclic fatigue crack growth rate decrease with decreasing load ratio and the threshold stress intensity factor ranges decrease with increasing load ratio. It is interesting that for the load ratio $R = 0.3$ and above about 10^{-9} m cycle^{-1}, the slope of the curve increases. The fatigue crack growth velocities, da/dt, are plotted in Fig. 5b against the sustained stress intensity factor, K_I for static loading and the maximum stress intensity factor, K_{max}, for cyclic loading. The broken lines show predicted static fatigue data based on the cyclic data. The correction is an overestimate because the load ratio has been used instead of the stress intensity factor ratio to calculate the correction. The crack growth rate increases with increasing load ratio. This is opposite to the behaviour found for ceramics at room temperature where reverse loading is more damaging [30, 33]. If the crack growth rates are dependent only on the peak stress intensity of the fatigue cycle and do not depend on the amount of unloading (characterized by R), crack growth curves obtained with different load ratios should tend to converge to a single curve when the cyclic crack growth curves are plotted as a function of K_{max} instead of ΔK. This is contrary to our results where even with an overestimate of the correction the data do not overlap. The results therefore indicate that the stress ratio plays a role in determining the crack growth rates.

3.4. Microscopic analysis

Fig. 6a shows a scanning electron micrograph of the fracture surface after a cyclic fatigue test at 1000 °C. The slow crack growth region is clearly apparent from the fast fracture region. Elongated β-sialon grains are clearly visible in Fig. 6b. The fracture behaviour under static loading showed similar features. Small particles produced by oxidation were apparent on the fracture surfaces. Their appearance and the test temperatures used suggests that the oxidation was not significant.

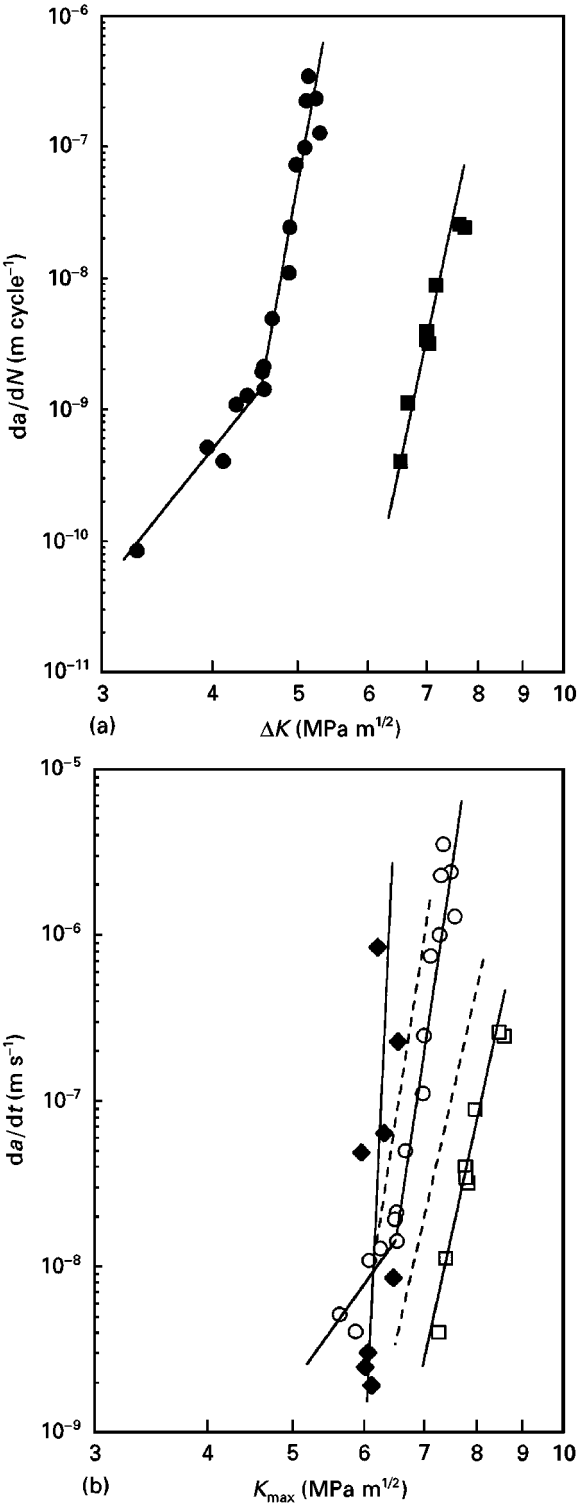

Figure 5 (a) Relationship between fatigue crack growth rate, da/dN, and stress intensity factor range, ΔK, for β-sialon ceramic subjected to cyclic tension loading at 1000 °C and cyclic frequency of 10 Hz and load ratios, $R = 0.1$ (■) and $R = 0.3$ (●). (b) Variation in crack growth velocity, da/dt, as a function of sustained stress intensity factor, K_I, for static crack growth ($R = 1$) in β-sialon ceramic at 1000 °C in air (◆). Also shown are the cyclic fatigue crack growth velocities, da/dt = (da/dN)f, as a function of the maximum stress intensity factor, K_{max}, for frequency, $f = 10$ Hz and load ratios, $R = 0.1$ (□) and $R = 0.3$ (○). The broken lines represent predicted static fatigue crack growth rate based on the cyclic fatigue data.

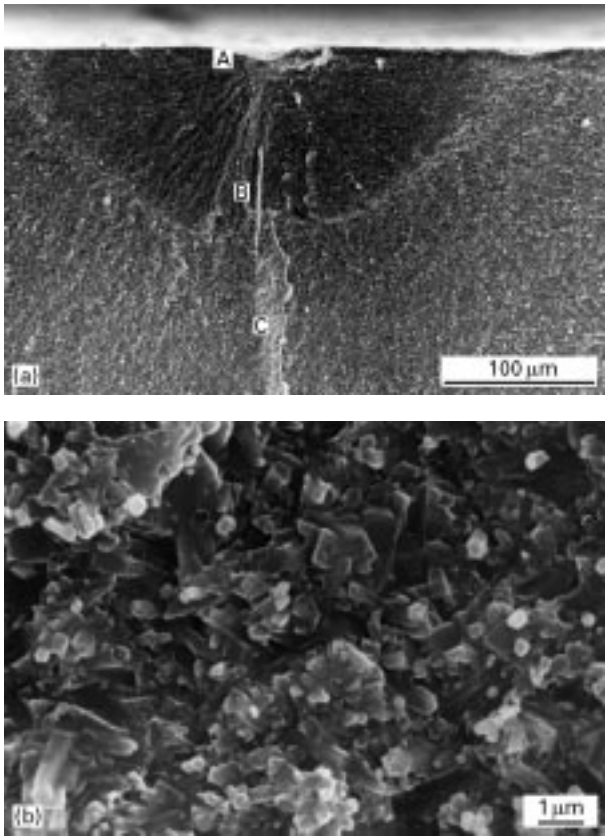

Figure 6 Scanning electron micrographs of the fracture surfaces a cyclic fatigue test at 1000 °C: (a) regions of slow and fast crack growth; (b) slow crack growth region showing pull-out whisker-like β-sialon.

3.5. Crack growth mechanisms

At ambient temperature, the basis for cyclic fatigue crack growth in ceramics is considered to be primarily associated with a progressive suppression of crack-tip shielding under cyclic loads behind the crack tip; the essential mechanism of crack advance at or ahead of the tip is assumed to be largely unchanged from that under quasistatic loading [30]. In silicon-nitride-based ceramics where toughening is introduced principally through the interlocking and bridging of grains between separating crack surfaces by having an elongated β-sialon grain structure [26], these whisker-like grains bridge the crack faces during the crack growth process and lead to significant improvements in fracture toughness. However, crack-wake contact through grain bridging leads to a different scenario in fracture behaviour under cyclic and static loads at room and high temperatures [5–15, 25–33]. At room temperature, cyclic fatigue can be associated with a progressive degradation of the whisker-like β-sialon grain bridging in the wake of the crack tip [26]. Some evidence for the operation of enhanced grain bridging and pull-out in the present ceramic at high temperatures is shown in Fig. 7. The effect of crack-tip shielding due to bridging of grains can be evaluated using the approach of Liu and Chen [6]. Besides both the applied stress intensity factor and the residual stress intensity factor, the effective stress intensity factor, K_{tip}, at the crack tip will be given by the relationship

$$K_{tip} = K_{app} + K_{res} + K_b \qquad (10)$$

where K_b is the reduction in stress intensity factor at the crack tip due to the bridging behind the crack tip and is therefore negative. According to Equation 10, because progressive deterioration of crack-wake

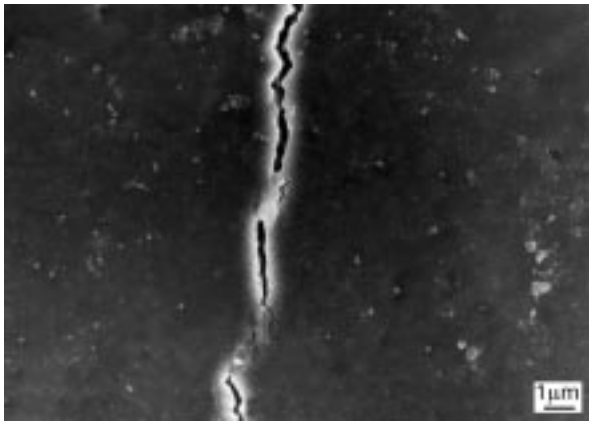

Figure 7 Cyclic fatigue crack growth path on the polished surface of a specimen after cyclic fatigue test at 1000 °C showing bridging by whisker-like β-sialon.

bridging occurs during cyclic fatigue owing to the repeated loading and unloading involved at room temperature, a reduction in crack-tip shielding under cyclic fatigue increases the crack growth compared with that under static loading. However, the opposite behaviour is found at high temperatures [8–20]. Fig. 3 shows that a significant increase in the crack growth rate occurs at 1000 °C compared with 900 °C and room temperature. This behaviour is probably a consequence of the softening of the amorphous grain-boundary phases, as suggested by Hansson *et al.* [20].

The evidence strongly suggests that the high-temperature fracture and fatigue behaviour of ceramics is determined by the viscous nature of the intergranular amorphous phases present in the materials. Silicon nitride materials are known to undergo a brittle-to-ductile transition at approximately 1000 °C [13]. Silicon nitride multiphase ceramics densified via liquid-phase sintering have been reported [27] to contain amorphous phases at triple grain junctions and grain boundaries which may be predominantly metal–Al–Si–O–N oxynitride glasses. Although the grain-boundary phases were predominantly crystallised in the present material, some of them also existed in the form of amorphous phase.

Viscous flow of the intergranular glass films can occur above the glass transition temperature to produce non-linear deformation. This enables several processes to occur which could influence fracture and fatigue behaviour. Grain-boundary sliding and cavitation could accommodate the strains in the region of crack tips and reduce the crack tip stress intensity factor [16]. The high stresses around crack tips probably explains why the creep damage can be significant there but not necessarily apparent as a gross creep deformation of the whole specimen, which was the case in this study. The presence of glass phase on the fracture surface can produce crack bridging ligaments [34]. In front of the crack tip the viscous flow of the intergranular glass phase can lead to enhanced cavitation and provide a mechanism for subcritical crack growth [35].

The slower crack growth rates under cyclic loading compared with static loading at high temperatures can be explained in terms of both the degradation of glassy crack bridging ligaments and the evolution of cavitation in front of the crack tip. Under static loading, the strength of the viscous ligaments will decay with time owing to relaxation caused by viscous flow. While under cyclic loading within appropriate regimes of temperature–viscosity and frequency–crack-opening rates the crack bridging forces can be much higher [34]. The closure forces produced by the ligaments is proportional to the viscosity of the glass and the crack-opening rate. Clearly there must be a limit to this behaviour. When the forces generated are relatively high and the ligaments cannot flow at a sufficient rate, they must brake. The ligaments may be repaired on reverse loading and this would give rise to a strong dependence of crack growth rate on load ratio, R, as observed in this study (Fig. 5a). Crack-tip cavitation would produce a similar fatigue crack growth behaviour and both processes may occur at the same time. Under static loading the sustained tensile stresses will be more effective than cyclic loading at producing cavitation damage ahead of the crack tip. The linking of these cavities and the easier crack path that they produce would enable stable incremental crack growth.

4. Conclusions

Based on a study of static and cyclic fatigue crack growth behaviour from Vickers indentation in Sm–β-sialon at temperatures from 25 to 1000 °C air, the following conclusions can be drawn.

1. An effective test method by multiple controlled Vickers flaws in four-point bending configuration was developed for measuring the fatigue crack growth rate of structural ceramics at high temperatures.

2. The cyclic fatigue crack growth behaviour at temperatures from 25 to 900 °C showed similar characteristics. However, a significantly lower cyclic fatigue crack growth threshold and higher crack growth rates were found at 1000 °C compared with those at room temperature.

3. An increase in cyclic frequency, from 1 to 10 Hz, caused a reduction of up to two orders of magnitude in crack propagation rates per cycle.

4. High-temperature cyclic fatigue crack growth rates increased with increasing load ratio.

Acknowledgements

The authors wish to thank Dr F. Guiu of the Department of Materials, Queen Mary and Westfield College, University of London, for helpful discussions. G.-D. Zhan was supported by a Royal Society K.C. Wang Fellowship.

References

1. A. G. EVANS and E. A. CHARLES, *J. Amer. Ceram. Soc.* **59** (1976) 371.
2. M. T. LAUGIER, *J. Mater. Sci. Lett.* **6** (1987) 355.
3. J. J. PETROVIC, L. A. JACOBSON, P. K. TALTY and A. K. VASUDEVAN, *J. Amer. Ceram. Soc.* **58** (1975) 113.

4. M. G. MENDIRATTA and J. J. PETROVIC, *ibid.* **61** (1978) 226.
5. S. Y. LIU, I.-Y. CHEN and T. Y. TIEN, *ibid.* **77** (1994) 137.
6. S. Y. LIU and I.-Y. CHEN, *Acta Mater.* **44** (1996) 2079.
7. G.-D. ZHAN, J.-L. SHI, T.-R. LAI and T.-S. YEN, *J. Eur. Ceram. Soc.* **17** (1997) 1267.
8. C.-K. JACK LIN, M. G. JENKINS and M. K. FERBER, *J. Eur. Ceram. Soc.* **12** (1993) 3.
9. G. D. QUINN, *J. Mater. Sci.* **25** (1990) 4361.
10. G. D. QUINN, *ibid.* **25** (1990) 4377.
11. C.-K. JACK LIN, M. G. JENKINS and M. K. FERBER, *ibid.* **29** (1994) 3517.
12. L. CHUCK, D. E. McCULLUM, N. L. HECHT and S. M. GOODRICH, *Ceram. Engng Sci. Proc.* **12** (1991) 509.
13. Y. MUTOH, K. YAMAISHI, N. MIYAHARA and T. OIKAWA, in "Fracture mechanism of ceramics", Vol. 10, edited by R. C. Bradt *et al.* (Plenum, New York, 1992) pp. 427–440.
14. U. RAMAMURTHY, A. S. KIM, S. SURESH and J. J. PETROVIC, *J. Amer. Ceram. Soc.* **76** (1993) 1953.
15. U. RAMAMURTHY, S. SURESH and J. J. PETROVIC, *ibid.* **77** (1994) 2681.
16. D. YAO and J.-K. SHANG, *ibid.* **77** (1994) 2911.
17. L. X. HAN and S. SURESH, *ibid.* **72** (1989) 1233.
18. L. EWART and S. SURESH, *J. Mater. Sci.* **27** (1992) 5181.
19. M. MASUDA, T. SOMA and M. MATSUI, *J. Eur. Ceram. Soc.* **6** (1990) 253.
20. T. HANSSON, Y. MIYASHITA and Y. MUTOH, in "Fracture mechanics of ceramics", Vol. 12, edited by R. C. Bradt *et al.* (Plenum, New York, 1996).
21. U. RAMAMURTHY, T. HANSSON and S. SURESH, *J. Amer. Ceram. Soc.* **77** (1994) 2985.
22. D. B. MARSHALL and B. R. LAWN, *ibid.* **63** (1980) 532.
23. J. C. NEWMAN Jr and I. S. RAJU, National Aeronautics and Space Administration Technical Paper 1578 (available from National Technical Information Service, Springfield, VA) (1979).
24. "Standard recommended practice for fracture testing with surface-crack tension specimens", ASTM Standard E 740-80, "ASTM Annual Book of Standards", Vol. 3.01, (American Society of Testing and Materials, Philadelphia, PA, 1983) pp. 740–750.
25. G.-D. ZHAN, J.-L. SHI, T.-R. LAI, T.-S. YEN, Y. ZHOU and Y.-Z. ZHANG, *J. Mater. Sci.* **31** (1996) 3535.
26. G.-D. ZHAN, J.-L. SHI, D.-Y. JIANG, F.-Y. WU, T.-R. LAI and T.-S. YEN, *ibid.* **31** (1996) 5045.
27. R. KOSSWSKY, *J. Amer. Ceram. Soc.* **56** (1973) 531.
28. M. TAKATSU, K. OHYA and M. ANDO, *J. Jpn. Ceram. Soc.* **98** (1990) 490.
29. R. H. DAUSKARDT, D. B. MARSHALL and R. O. RITCHIE, *J. Amer. Ceram. Soc.* **73** (1990) 893.
30. M. J. REECE, F. GUIU and M. F. R. SAMMUR, *ibid.* **72** (1989) 348.
31. R. O. RITCHIE and R. H. DAUSKARDT, *J. Jpn. Ceram. Soc.* **99** (1991) 1047.
32. M. OKAZAKI, A. J. McEVILY and T. TANAKA, *Metall. Trans. A* **22** (1991) 1425.
33. S. HORIBE, *J. Eur. Ceram. Soc.* **6** (1990) 89.
34. U. RAMAMURTHY, *J. Amer. Ceram. Soc.* **79** (1996) 945.
35. K. S. CHAN and R. A. RAGE, *ibid.* **76** (1993) 803.

Received 8 July 1997
and accepted 11 May 1998